POLITECNICO DI TORINO
Repository ISTITUZIONALE

Robust optical frequency dissemination with a dual-polarization coherent receiver

(Article begins on next page)

05 May 2024

Robust optical frequency dissemination with a dual-polarization coherent receiver

Cecilia Clivati,[1,*] ⓘ **Paolo Savio,**[2] ⓘ **Silvio Abrate,**[2] **Vittorio Curri,**[3] ⓘ **Roberto Gaudino,**[3] **Marco Pizzocaro,**[1] **and Davide Calonico**[1]

[1]*Istituto Nazionale di Ricerca Metrologica INRIM, strada delle cacce 91, 10135 Torino, Italy*
[2]*Fondazione LINKS, 10135 Torino, Italy*
[3]*Politecnico di Torino, Dipartimento Elettronica e Telecomunicazioni, c.so Duca degli Abruzzi 24, 10135 Torino, Italy*
[*]*c.clivati@inrim.it*

Abstract: Frequency dissemination over optical fiber links relies on measuring the phase of fiber-delivered lasers. Phase is extracted from optical beatnotes and the detection fails in case of beatnotes fading due to polarization changes, which strongly limit the reliability and robustness of the dissemination chain. We propose a new method that overcomes this issue, based on a dual-polarization coherent receiver and a dedicated signal processing that we developed on a field programmable gated array. Our method allowed analysis of polarization-induced phase noise from a theoretical and experimental point of view and endless tracking of the optical phase. This removes a major obstacle in the use of optical links for those physics experiments where long measurement times and high reliability are required.

1. Introduction

In recent years, the dissemination of frequency references over phase-stabilised optical fibers has become a key tool in a number of physics areas. In fundamental metrology, it enabled remote atomic clock comparisons at their ultimate level, overcoming the resolution of satellite-based techniques by more than 3 orders of magnitude [1–4]. Phase-stabilised optical links have also been used in high-resolution atomic and molecular spectroscopy [5–7], radioastronomy and space geodesy based on Very Long Baseline Interferometry (VLBI) [8–10], and to detect seismic noise in seas and oceans, one of the most challenging tasks of modern seismology [11].

Coherent frequency dissemination over fiber is based on the transmission of a continuous wave, unmodulated optical carrier from a National Metrology Institute to the user laboratory. The optical signal is a sub-Hz-linewidth laser emitting in the 1550 nm region, whose frequency is measured with high accuracy against an atomic clock. The ultrastable laser is sent to the remote laboratory using standard telecom optical fibers, possibly shared with other network clients, and here used as the local frequency reference. To preserve the phase-coherence between the launched and received signal, the phase-variations imposed to the carrier by mechanical stresses of the fiber are cancelled using the Doppler-noise-stabilization technique [12]. Such technique has been successfully demonstrated over distances up to 2000 km [13] and there is now interest in developing robust and more flexible infrastructures [14].

As fiber-based frequency dissemination reaches maturity, fundamental limitations are being investigated [15], and existing implementations are striving for increased robustness and service uptime. Far from being a mere operational requirement, the latter is a key step to enable a new class of physics experiments, where the high measurement precision allowed by frequency dissemination over fiber can be combined with averaging times of several hours or days. This could open new possibilities, for instance, in fundamental physics experiments: nowadays the most advanced tests of special relativity [2] and the search for dark matter [16] rely on fiber-based

clocks comparisons over daily scales. In applied sciences such as VLBI geodesy and seismic detection, the potential of fiber-based frequency dissemination can be fully disclosed once uninterrupted operation is demonstrated.

Frequency dissemination over fiber is based on the precise measurement of the phase difference between the local and fiber-delivered laser sources, which is extracted from optical beatnotes. Their reliable detection is then among the most critical aspects. The time-varying stresses to which the fiber is exposed affect not only the phase, but the polarization of the transmitted signal as well. On long timescales they are mostly caused by temperature changes, while on shorter times external electromagnetic fields [17,18], acoustic noise and human intervention play a significant role [19]. This latter in particular may happen on timescales of fractions of seconds and have large entity, up to krad/s. Polarization changes make the power of the detected beatnotes vary in time. When the signal to noise ratio (SNR) at detection drops below a certain threshold, temporary losses of phase-coherence can occurr (cycles slips), which affect the ultimate link accuracy. In the worst case, when the two interfering lasers have orthogonal polarizations, the beatnote completely fades and the phase information is no longer retrieved, causing failure of the whole system. We observed such events while operating our four-segment >1700 km fiber link in Italy [8,20,21]. The link is established on a shared backbone, in which network operators have access to fiber housings and network nodes for maintenance and upgrade. While for most time polarization drifts over hourly scales due to temperature excursions, we observed sudden flips from time to time, especially in diurnal hours, which we attributed to human work along the line. Similar effects are encountered on aerial optical fibers, which are strongly exposed to environmental noise such as wind and magnetic fields [18,22].

To cope with such issues, it is possible to automatically adjust the signal's polarization to maximise the beatnote power at detection. Polarization variations can be induced mechanically, for instance by twisting or locally heating the fiber. In this case, the response time can be as long as hundreds of millisecond. Fiber squeezers or electro-optic polarization controllers are much faster, with a response time of tens of microseconds. However, even with such actuators, the beatnote power can be recovered in tens of milliseconds, and failures still happen in the case of fast or large polarization variations such as those induced by human intervention. A faster, failure-free active control is not straightforward [23], since it relies on an optimization, non-deterministic algorithm, and the actuator response strongly depends on the local state of the signal's polarization.

Here we propose an alternative approach, based on a dual-polarization coherent receiver, or optical hybrid, associated to digital signal processing. This technology is already in use in all long-haul optical transmission systems based on quadrature amplitude modulation formats [24]. The currently achieved bit rate of 400 Gb/s per wavelength already relies on polarization-multiplexing and the progressive increase in the transmission speed requirements will need higher-order modulation formats. In such solutions, the optical hybrid is a standard integrated component, now commercialised by most telecom manufacturers.

We introduce this device in a metrological context and use it for low-noise tracking of an optical signal's phase and polarization. Such tasks cannot be achieved with commonly-used phase-detectors based on a single photodiode. On one side, a single photodiode does not permit a unique determination of the signal's polarization state, as this task requires the decomposition of the signal in at least two orthogonal states of polarization. On the other side, phase-detection on a single photodiode fails when the signal and local oscillator generating the beatnote have orthogonal polarization, as in this case interference is lost.

The optical hybrid separates the signal and local oscillator into orthogonal components, enabling beatnotes to be detected along each axis separately. With a dedicated signal processing, we were able to extract the optical signal's phase, as well as its amplitude and polarization, regardless of the mutual polarization of the interfering beams.

So far, the problem of birefringence and polarization-induced phase noise in coherent fiber optic systems has been analysed almost exclusively in the telecommunication community. Here, the focus was on theoretical and computational aspects for optimal phase-recovery [25]. We provide an experimental study and quantify, for the first time to our knowledge, its impact in metrological optical links. To this purpose, it was necessary to adapt existing models that describe the effect of fiber birefringence in telecomunications to the metrological context. Then, we modelled the optical hybrid response and developed a dedicated algorithm to retrieve the phase information, which is the quantity of main interest. We used the device in a real-field environment, composed by 50 km of metropolitan optical fiber deployed around the city of Turin, Italy, and compared its performances to those of a usual detection scheme based on a photodiode.

Our results show that the proposed detection scheme is a viable solution in fiber-based frequency dissemination, allowing long-term operation of optical links while preserving the metrological requirements in terms of resolution. This allows an improvement in the reliability and reduces the risk of unexpected losses of coherence. In addition, the developed signal processing, being based on a Field Programmable Gated Array (FPGA), can be readily adapted to more complex tasks and improve monitoring capabilities, autonomous relocking and cycles-slips detection.

The paper is organised as follows: Sec. 2 explains the model we developed to describe fiber birefringence in the metrological context; Sec. 3 shows the optical hybrid principle of operation and Sec. 4 reports on the obtained experimental results.

2. Polarization in optical fibers

The effect of birefringence in an optical fiber can be analysed using the Jones calculus [26]. In this formalism the electric field representing the signal propagating through a single mode fiber is described in terms of phase and polarization by a two-component vector:

$$E_{\text{in}} = E_0 \begin{bmatrix} E_{\text{in,x}} \\ E_{\text{in,y}} \end{bmatrix} e^{j(\omega t + \varphi_0)} \ , \ |E_{\text{in,x}}|^2 + |E_{\text{in,y}}|^2 = 1 \tag{1}$$

where ω is the optical angular frequency, φ_0 is a constant phase, and $E_{\text{in, x}}$, $E_{\text{in, y}}$ are the field components along orthogonal axes in a Cartesian $x - y$ reference frame. Any optical element interacting with the beam is modelled by a 2×2 matrix F, so that after interaction the resulting electric field is

$$E_{\text{out}} = F E_{\text{in}} \tag{2}$$

The effect of attenuation is not considered in this context, as coherent phase detection systems are not sensitive to the absolute power of the received signals.

Various expressions can be found in the literature for the Jones matrix of a single mode fiber [24]. In general, it can be described by a sequence of birefringent elements with random orientation [27]. Each element is characterised by two orthogonal principal axes oriented at an angle θ_i with respect to the x axis. The phase-delay accumulated by the optical carrier traversing it with polarization along one or the other principal axis differs by δ_i, which thus represents the element birefringence. In addition, each element also adds a phase-delay which is the same for both polarizations, $\varphi_{\text{f,i}}$. The Jones matrix of a birefringent element is unitary and has the form:

$$F_i = \begin{bmatrix} \cos\theta_i & -\sin\theta_i \\ \sin\theta_i & \cos\theta_i \end{bmatrix} \begin{bmatrix} e^{-j\delta_i/2} & 0 \\ 0 & e^{j\delta_i/2} \end{bmatrix} \begin{bmatrix} \cos\theta_i & \sin\theta_i \\ -\sin\theta_i & \cos\theta_i \end{bmatrix} e^{j\varphi_{\text{f,i}}}, \tag{3}$$

where δ_i, θ_i, and $\varphi_{\text{f,i}}$ change over time. According to the Jones formalism, the overall fiber can be described by the product of each element. The resulting matrix is still unitary and thus can be

written as:

$$F = \prod_{i=1}^{N} F_i$$

$$= \begin{bmatrix} \cos\theta & -\sin\theta \\ \sin\theta & \cos\theta \end{bmatrix} \begin{bmatrix} e^{-j\delta/2} & 0 \\ 0 & e^{j\delta/2} \end{bmatrix} \begin{bmatrix} \cos\theta & \sin\theta \\ -\sin\theta & \cos\theta \end{bmatrix} e^{j\varphi_f}. \tag{4}$$

δ and θ represent the overall fiber birefringence, while $\varphi_f = \sum_{i=1}^{N} \varphi_{f,i}$ represents the optical length, which can vary either due to a geometric expansion of the fiber or a change in the fiber refractive index.

In bidirectional optical links for frequency dissemination, part of the signal reaching the remote fiber end is reflected back for phase-noise cancellation. Typically, a Faraday mirror is used, whose Jones matrix is $M = [[0, 1], [-1, 0]]$. The expression of the round-trip field is:

$$E_{rt} = F^T M F E_{in} = E_0 \begin{bmatrix} E_{in,y} \\ -E_{in,x} \end{bmatrix} e^{j(\omega t + \varphi_0 + 2\varphi_f)}, \tag{5}$$

under the assumption that birefringence changes on timescales which are much longer than the round-trip time. This is justified as the latter amounts to 1 ms for a 100 km link. It can be seen that E_{rt} is orthogonal to the launched field and insensitive to the fiber birefringence. The use of a Faraday mirror avoids beatnote fading at the local end, ensuring endless tracking of the link's phase noise. The round-trip accumulated phase $2\varphi_f$, which is common for both birefringence axes, is then stabilised by the Doppler noise cancellation system. In this configuration, Eq. (2) and Eq. (4) still hold, with the only difference that within the loop bandwidth, $\varphi_f \approx 0$.

At the link remote end, the incoming light is usually compared to an optical local oscillator (LO) E_{lo} on a photodiode. The photocurrent produced by the two interfering beams on the photodiode can be written in terms of the fields components as:

$$I_{pd} = I_0 \langle |E_{out} + E_{lo}|^2 \rangle$$

$$= I_0 \left(2\mathfrak{R}[E_{out,x}E_{lo,x}^*] + 2\mathfrak{R}[E_{out,y}E_{lo,y}^*] \right) \tag{6}$$

where I_0 is a constant factor, and we neglected non-oscillating terms which do not contribute to the beatnote.

The two terms can interfere constructively or destructively depending on the fiber birefringence, making amplitude and phase of the photodiode signal to vary consequently.

In principle, information about phase and polarization of incoming light could be retrieved if phase and amplitude of the beatnotes on the x and y axes are analysed separately. This could be done, for instance, with a polarizing beamsplitter cube and a couple of photodiodes. However, this setup is never used in practice as it adds complexity to the experimental apparatus by introducing bulk optical components and requires non trivial signal processing. The optical hybrid, on the contrary, is a fully integrated, alignment-free device that implements this approach, allowing more advanced detection schemes.

3. Phase detection with an optical hybrid

The functional scheme of the device is shown in Fig. 1. The input field is decomposed in its $E_{out,x}, E_{out,y}$ components by a polarizing beam splitter cube, then further split into two parts. The LO field, assumed linearly polarized, is brought to the optical hybrid with a polarization-maintaining fiber and split into two equal components along the x and y directions: $E_{lo} = E_{lo,0}[1/\sqrt{2}, 1/\sqrt{2}]e^{j(\omega_{lo}t + \varphi_{lo})}$. Each component is further separated into two parts, one

phase-delayed by $\pi/2$ with respect to the other, and interfered with the signal. This latter step allows separate detection of the in-phase (I_1 and I_3) and quadrature (I_2 and I_4) beatnote components along each axis, and is crucial to retrieve the amplitude information. The beatnotes are detected with four balanced photodiodes.
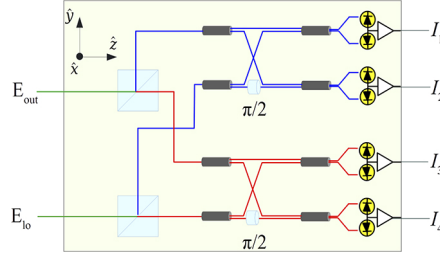

Fig. 1. A sketch of a dual polarization coherent receiver. Red and blue paths indicate the two orthogonal components of local (E_{lo}) and fiber-delivered (E_{out}) optical fields. The beatnotes are detected with four balanced photodiodes.

The currents produced by the optical hybrid can be written as:

$$
\begin{aligned}
\frac{I_1}{I_0} &= 2\Re[E_{\mathrm{out,x}}E_{\mathrm{lo,x}}^*] \\
\frac{I_2}{I_0} &= 2\Im[E_{\mathrm{out,x}}E_{\mathrm{lo,x}}^*] \\
\frac{I_3}{I_0} &= 2\Re[E_{\mathrm{out,y}}E_{\mathrm{lo,y}}^*] \\
\frac{I_4}{I_0} &= 2\Im[E_{\mathrm{out,y}}E_{\mathrm{lo,y}}^*]
\end{aligned}
\tag{7}
$$

With this set of observables, it is possible to determine the phase and polarization of incoming light independently when proper signal processing is implemented.

In Subsec. 3.1, 3.2 and 3.3 we propose some cases which illustrate important aspects of the problem. On one side we show how the combined processing of the four signal improves phase detection over that achievable with a single photodiode. On the other side, we point out a subtle and often overlooked problem in low-noise phase-detection, i.e. the ambiguity which exist between phase and birefringence and how the two aspects cannot be distinguished in some particular configurations.

3.1. A linearly-polarized beam through a generic birefringent element.

Let us consider a linearly-polarized optical field with 45° orientation in the x, y-plane, travelling through a fiber and interfering with a LO having 45° orientation in the x, y-plane. For simplicity, it is convenient to assume that both fields are normalised to 1, i. e.: $E_{\mathrm{in}} = [1/\sqrt{2}, 1/\sqrt{2}]e^{j(\omega t+\varphi_0)}$, and $E_{\mathrm{lo}} = [1/\sqrt{2}, 1/\sqrt{2}]e^{j(\omega_{\mathrm{lo}}t+\varphi_{\mathrm{lo}})}$. Using Eqs. (2), (4) and (7), the photocurrents produced by

the optical hybrid can be written as:

$$\frac{I_1}{I_0} = 2\sqrt{2}\sin\frac{\delta}{2}\sin\theta\cos(\theta+\pi/4)\sin(\varphi) + \cos\left(\varphi - \frac{\delta}{2}\right)$$

$$\frac{I_2}{I_0} = -2\sqrt{2}\sin\frac{\delta}{2}\sin\theta\cos(\theta+\pi/4)\cos(\varphi) + \sin\left(\varphi - \frac{\delta}{2}\right)$$

$$\frac{I_3}{I_0} = 2\sqrt{2}\sin\frac{\delta}{2}\sin\theta\sin(\theta+\pi/4)\sin(\varphi) + \cos\left(\varphi + \frac{\delta}{2}\right)$$

$$\frac{I_4}{I_0} = -2\sqrt{2}\sin\frac{\delta}{2}\sin\theta\sin(\theta+\pi/4)\cos(\varphi) + \sin\left(\varphi + \frac{\delta}{2}\right)$$

(8)

where $\varphi = (\omega - \omega_{\text{lo}})t + \varphi_0 + \varphi_{\text{f}} - \varphi_{\text{lo}}$ is the information of interest. This contains the phase difference between local and remote laser, including the residual contribution of the optical fiber. We recall that this latter term is ideally $\varphi_{\text{f}} \approx 0$ if Doppler noise cancellation is activated. The photocurrent produced by a single photodiode in absence of a beamsplitter cube can be computed as $I_{\text{pd}} = I_1 + I_3$. It is instructive to look at some particular cases.

If $\theta = 0$, the signal produced by a single photodiode is $I_{\text{pd}} = 2I_0\cos\frac{\delta}{2}\cos\varphi$: the beatnote phase is not affected by birefringence, however the amplitude varies according to δ, vanishing for $\delta = (2n+1)\pi$, with n integer. With an optical hybrid, instead, it is always possible to retrieve δ and φ separately by combining I_1, I_2, I_3, and I_4.

Posing $\theta = \pi/4$ we analyse the case in which one of the principal axes of the birefringent element is oriented on the same direction as the input field. The photocurrents produced by the optical hybrid simplify to:

$$\frac{I_1}{I_0} = \cos\left(\varphi - \frac{\delta}{2}\right)$$

$$\frac{I_2}{I_0} = \sin\left(\varphi - \frac{\delta}{2}\right)$$

$$\frac{I_3}{I_0} = \cos\left(\varphi - \frac{\delta}{2}\right)$$

$$\frac{I_4}{I_0} = \sin\left(\varphi - \frac{\delta}{2}\right)$$

(9)

and similarly, that produced by a single photodiode: $I_{\text{pd}} = 2I_0\cos\left(\varphi - \frac{\delta}{2}\right)$.

In such a configuration the birefringent element acts as a pure phase modulator. Any variation in δ does not affect the output polarization which remains linear, but produces a shift in the output phase. This exemplifies the ambiguous case in which φ and δ cannot be distinguished on the output field either using an optical hybrid or a single photodiode. In addition, we note that return light, reflected by a Faraday mirror, is shifted by an opposite amount $+\delta/2$ and as a result the round-trip signal is not affected by birefringence. While φ is detected and stabilised by the Doppler noise cancellation, no control is possible on δ. Thus, the output signal is still affected by residual noise which ultimately limits the achievable frequency stability.

3.2. A circularly-polarized beam through a $\lambda/2$ waveplate.

If the input beam is circularly-polarised, i.e. $E_{\text{in}} = [1/\sqrt{2}e^{j\pi/2}, 1/\sqrt{2}]e^{j(\omega t + \varphi_0)}$, the photocurrents produced by the optical hybrid in presence of a generic birefringent element become:

$$\frac{I_1}{I_0} = 2 \sin \frac{\delta}{2} \sin \theta \sin(\varphi - \theta) - \sin\left(\varphi - \frac{\delta}{2}\right)$$

$$\frac{I_2}{I_0} = -2 \sin \frac{\delta}{2} \sin \theta \cos(\varphi - \theta) + \cos\left(\varphi - \frac{\delta}{2}\right)$$

$$\frac{I_3}{I_0} = 2 \sin \frac{\delta}{2} \sin \theta \cos(\varphi - \theta) + \cos\left(\varphi + \frac{\delta}{2}\right)$$

$$\frac{I_4}{I_0} = 2 \sin \frac{\delta}{2} \sin \theta \sin(\varphi - \theta) + \sin\left(\varphi + \frac{\delta}{2}\right)$$

(10)

Let us consider a particular case in which the birefringent element is a $\lambda/2$ waveplate with arbitrary orientation. In this case $\delta = \pi$ and Eq. (10) simplify to:

$$\frac{I_1}{I_0} = \cos(\varphi - 2\theta)$$

$$\frac{I_2}{I_0} = \sin(\varphi - 2\theta)$$

$$\frac{I_3}{I_0} = -\sin(\varphi - 2\theta)$$

$$\frac{I_4}{I_0} = \cos(\varphi - 2\theta)$$

(11)

From these equations it is impossible to distinguish a variation in φ from a variation in θ just by looking at the output field components. This ambiguity can be intuitively explained as follows. As expected when a $\lambda/2$ waveplate is rotated by an angle $\Delta\theta$, the electric field components are rotated consequently by an angle $2\Delta\theta$. Since the input polarization is circular, the output polarization remains circular as well. However, the output field is rotated. This rotation has on the output field the same effect as a phase shift $\Delta\varphi = -2\Delta\theta$. It is easily verified that the same ambiguity is observed either with an optical hybrid or a single photodiode. Similarly to the case described in Sec. 3.1 a residual noise, this time depending on θ, affects the output field even if Doppler noise stabilisation is activated.

3.3. A circularly-polarized beam through a $\lambda/4$ waveplate.

Consider now the case in which a circularly-polarised beam enters a $\lambda/4$-waveplate ($\delta = \pi/2$) with arbitrary orientation. Equation (10) simplify in this case to:

$$\frac{I_1}{I_0} = \sqrt{2} \sin\left(\theta - \frac{\pi}{4}\right) \sin\left(\varphi - \theta - \frac{\pi}{4}\right)$$

$$\frac{I_2}{I_0} = -\sqrt{2} \sin\left(\theta - \frac{\pi}{4}\right) \cos\left(\varphi - \theta - \frac{\pi}{4}\right)$$

$$\frac{I_3}{I_0} = -\sqrt{2} \cos\left(\theta - \frac{\pi}{4}\right) \sin\left(\varphi - \theta - \frac{\pi}{4}\right)$$

$$\frac{I_4}{I_0} = \sqrt{2} \cos\left(\theta - \frac{\pi}{4}\right) \cos\left(\varphi - \theta - \frac{\pi}{4}\right)$$

(12)

and the signal produced by a single photodiode to: $I_{\text{pd}} = -2I_0 \cos(\theta) \sin\left(\varphi - \theta - \frac{\pi}{4}\right)$. The output field is linearly polarised, with orientation depending on θ, and the phase is affected as well. With a single photodiode this ambiguity cannot be solved and, even more important, detection fails completely when $\theta = (2n + 1)\pi/2$.

With an optical hybrid, a power drop in the beatnote detected on two of the four photodiodes is always compensated by an increase on the other two. Hence, information is never lost. In

addition, separation of θ and φ is possible by combining the phase and amplitude information from the four of them.

The examples described in Secs. 3.2 and 3.3 can be easily realised in an experimental setup, using standard optical components. Sec. 4 will show the obtained results.

4.   Experimental results

We used an optical hybrid to detect the phase difference between the signal received from a phase-stabilised optical link and a local oscillator and phase lock the two, and compare its performance with a standard detection scheme based on a single photodiode.

The setup is shown in Fig. 2. A narrow-linewidth laser (Master Laser) with 2×10^{-15} frequency instability at 1 s is generated by frequency locking a diode laser to a high-finesse Fabry-Pérot cavity [28], then sent through an optical fiber link to a remote station. About 1 mW of optical power is injected in the system. The link is established on a 50 km-long fiber deployed around the city of Turin and is part of the backbone for coherent frequency dissemination we developed in Italy [20]. Two parallel fibers, each 25 km long, are connected at the far end to realise a loop with both ends in our laboratory. This enables us to phase-compare the launched and received signal. The link losses amount to 25 dB, therefore an Erbium-doped Fiber Amplifier is used along the path. The metropolitan fiber can be excluded from the setup and replaced by a short patchcord to analyze the ultimate noise floor of the system. Just before injection in the fiber loop we inserted a free-space-path that enables us to modify the launched signal's polarization state. In principle, there is no preferred state of polarization. We chose to operate with circular input polarization, as this configuration allows implementation of the examples described in Secs. 3.2 and 3.3 with standard optical components. The input field polarization was adjusted before any experimental run by sliding in the free-space path a block composed by a beam splitter cube with two photodiodes and by analysing the reflected and transmitted power with a set of $\lambda/4$ and $\lambda/2$ waveplates. We inserted a manual polarization controller at the fiber output to modify the fiber birefringence on purpose. The link is phase stabilised using the Doppler noise cancellation technique: part of the radiation reaching the remote fiber end is reflected back to the local end using a Faraday mirror and here compared to a portion of the original light used as a reference. This allows detection of the round-trip fiber noise, which is actively compensated by acousto-optic modulator AOM1. At the remote end, AOM2 applies a fixed frequency shift to distinguish spurious backreflections occurring along the link from the round-trip signal. The incoming light is split into two parts and used as a reference for phase-locking the diode lasers Slave Laser 1 and Slave Laser 2 at an offset frequency of 10 MHz.

The beatnote between the reference light and Slave Laser 1 is detected with an optical hybrid. The signals produced by the four photodiodes are sampled with a four-channel, 14-bit 125 MS/s analog to digital converter LTC2175-14 (by Analog Devices). The sampled signals are then sent to a Xilinx Kintex FPGA board which performs all the required digital signal processing. First, it down-mixes the sampled signals to DC with a digital local oscillator at 10 MHz and downsamples the result to around 500 kS/s. Then, it evaluates δ, θ, and φ by linearizing and inverting Eq. (10). Since linearization holds locally, at every step we evaluate the increments with respect to the previous solution. Even if initial values for δ, θ, and φ are chosen arbitrarily, iteration of the process ensures that the retrieved values converge to the expected ones after less than 10 steps. This approach relies on the assumption that phase and birefringence changes are continuous and slow as compared to the 500 kS/s sampling rate. This is justified, as they are of mechanical origin. The retrieved phase φ is then passed to a 20-bit digital-to-analog converter and used in a phase-locked loop (PLL) which acts on Slave Laser 1 input current.

The PLL between the reference light and Slave Laser 2 is implemented with analog electronics: the beatnote between the two is detected with a photodiode and the phase difference is extracted by an analog mixer in quadrature condition. We use a prescaler with a division factor of 10 to
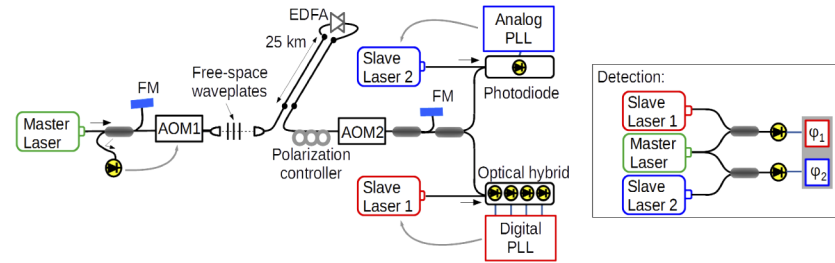
Fig. 2. Experimental setup: the Master Laser is sent through a phase-stabilised fiber with both ends inside the laboratory (EDFA: Erbium-doped Fiber Amplifier). At the link end, part of the light is back-reflected using a Faraday Mirror (FM) for phase stabilization. Acousto-optic modulator AOM1 is used to compensate the fiber noise; AOM2 is used as a fixed frequency shifter. Free-space waveplates allow setting of input signal polarization and a manual polarization controller is used to modify birefringence on purpose. At the link end, the beatnote between the incoming light and Slave Laser 1 is detected with an optical hybrid, and processed with digital electronics. The beatnote and PLL between Slave Laser 2 and the incoming light is performed on a single photodiode. Inset: part of the Master Laser is compared to Slave Laser 1 or Slave Laser 2 to measure out-of-loop phase noise φ_1 and φ_2.

extend the mixer's dynamic range. The phase difference is then sent to a Proportional-Integrative controller which acts on Slave Laser 2 input current.

All beatnotes are filtered with identical, 2 MHz-wide bandpass filters. Slave Laser 1 and Slave Laser 2 are then compared to the Master Laser on two additional photodiodes to assess the residual phase-noise (φ_1 and φ_2) in the two cases.

We performed a series of tests aimed at assessing the performances of the optical hybrid and the validity of our model and compared the results achieved with this device to those of a traditional detection scheme based on a single photodiode in a real-field environment. The results are reported in Subsec. 4.1, 4.2 and 4.3.

4.1. Characterization of the optical hybrid

In a first test we characterised the noise floor of the optical hybrid. For this test, the fiber loop was composed by a short piece of phase-stabilised fiber inside our laboratory. The four electrical signals at 10 MHz were processed by the FPGA to compute the error signal for locking Slave Laser 1 to the incoming light. In addition, we independently sampled the phase of each individual beatnote produced by the optical hybrid on a dead-time-free phase counter. Figure 3(a), panels A to C, shows δ, θ and φ as retrieved by the FPGA; the latter is used for the PLL.

In panel D, blue line labelled (1) shows the difference between the in-phase and quadrature component along the same axis (I_1 and I_2 with reference to Eq. (10)). The magenta line labelled (2) shows the difference between the two in-phase components on orthogonal axes (I_1 and I_3 with reference to Eq. (10)). As expected, the former is rather constant over time. The fractional frequency instability calculated from such phase measurement and scaled to the optical domain is shown in terms of the Allan deviation in Fig. 3(b) (labelled (1), blue line). This represents the statistical uncertainty associated to detection on the in-phase or quadrature port of the optical hybrid and can be considered as the noise floor, limited by the detection electronics. Instead, some discrepancy is observed between the two in-phase components, which quantifies the lower limit to polarization-induced phase noise. The periodic disturbance at around 500 s is attributed to the temperature cycles of amplitude ≈ 0.3 K caused by the air conditioning system inside our laboratory. The corresponding Allan deviation, shown in Fig. 3(b) (labelled (2), magenta line), indicates that birefringence can contribute a minimum instability at the 10^{-20} level even
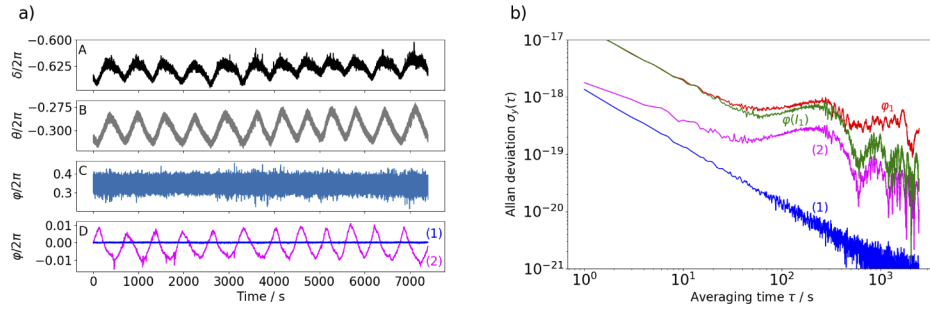
Fig. 3. Characterisation of the optical hybrid noise floor on a few-meters long optical link. (a) Panel A to C: the values of δ, θ and φ as retrieved by the FPGA connected to the optical hybrid. Panel D: blue line (1), difference between the in-phase and quadrature component along the same axis; magenta line (2), difference between two in-phase components along x and y axes. (b) Corresponding frequency instabilities. Blue line (1) and magenta line (2), as in (a); green line ($\varphi(I_1)$), phase detected by a single photodiode of the optical hybrid; red line (φ_1): out of loop phase between Slave Laser 1 and Master Laser.

on a few-m long fiber. The green trace labelled $\varphi(I_1)$ in Fig. 3(b) shows the instability of the beatnote as detected by a single photodiode of the optical hybrid. This measurement quantifies any difference between the phase φ estimated by the FPGA and stabilised by the PLL, and the phase detected by a photodiode, which is affected by birefringence according to Eq. (10). It also includes contribution of locking electronics, thus representing the upper limit to both effects. For comparison, the red trace labelled φ_1 in Fig. 3(b), shows the instability of the out-of-loop comparison between Slave Laser 1 and the Master Laser. The 3×10^{-19} instability floor observed on the long term is attributed to the short fibers of the interferometer which are not included in the phase-stabilised path. In all cases, the beatnote frequency averaged over the full duration of the measurement corresponded to the expected value within the measured instability.

These measurements show that the device has a negligible noise floor and poor sensitivity to environmental noise, and is adequate for high-resolution phase-detection in a metrological setup.

4.2. Birefringence-induced phase noise with fixed waveplates: validating the model

In a second experiment we inserted fixed elements of known birefringence in the fiber loop. We then examined the residual phase noise of the two PLLs and compared the results to the predicted behaviour. This enabled us to assess the validity of the model proposed in Sec. 3 and verify the arising of polarization-induced phase noise in specific experimental conditions, even in the presence of Doppler noise cancellation. For these tests, the fiber loop was composed by a short piece of phase-stabilised fiber inside our laboratory.

First, we implemented the example described in Sec. 3.2. We inserted a $\lambda/2$-waveplate in the optical path and rotated it at constant speed to perform 10 complete turns ($\Delta\theta = -20\pi$) in about 80 s. Figure 4 panels A (black line) and B (gray line) show δ and θ as recovered by the optical hybrid. Figure 4 panel C (red line) shows the phase of the out-of-loop beatnote between Slave Laser 1 and the Master Laser, φ_1; Fig. 4 panel D (blue line) shows the phase of the out-of-loop beatnote between Slave Laser 2 and the Master Laser, φ_2. Phase variations on these measurements associated to the waveplate rotation quantify the arising of polarization-induced phase noise with optical-hybrid and single photodiode detection schemes. While δ and θ exhibit small fluctuations, indicating that the optical hybrid does not recognise any variation in the polarization state of the output field, φ_1 increments by $\Delta\varphi = 40\pi$. The same happens on φ_2. This reflects the ambiguity described in Sec. 3.2 and shows experimentally how birefringence introduces phase noise to the

system which cannot be compensated by the Doppler noise stabilisation, both when detection is performed with the optical hybrid or with a single photodiode.
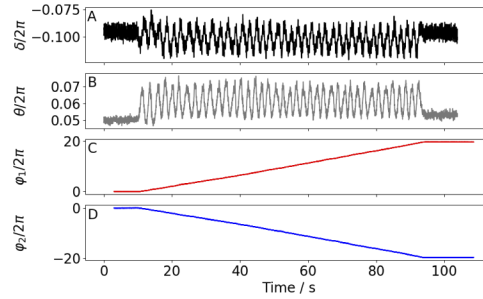

Fig. 4. Experimental results obtained with a circularly-polarised beam through a $\lambda/2$ waveplate ($\Delta\theta = -20\pi$). A (black) and B (gray): δ and θ retrieved by the FPGA with the optical hybrid; C (red): phase of the out-of-loop beatnote between Master Laser and Slave Laser 1, locked to the incoming light using the optical hybrid; D (blue): phase of the out-of-loop beatnote between Master Laser and Slave Laser 2, locked to the incoming light using a single photodiode.

The small fluctuations observed on δ and θ are associated to non-ideal behaviour of the waveplate or to non-perfect circularity of the input field polarization. We note that in the implementation of this setup, the optical fiber patches between the rotating waveplate and the optical hybrid add a constant birefringence to the system which is not considered in Eq. (11). However, this simply adds an offset in δ and θ as read by the optical hybrid.

We repeated this experiment with a rotating $\lambda/4$-waveplate, implementing the example described in Sec. 3.3. Equation (12) describe the expected output in presence of a rotating $\lambda/4$-waveplate, when no further birefringence is introduced after it. Figure 5 shows the calculated results: the phase recovered using a photodiode (shown in Panel D) is expected to increase linearly with $\Delta\varphi = -\Delta\theta$ as the waveplate rotates, while the optical-hybrid-based approach (Panel C) solves the problem correctly.
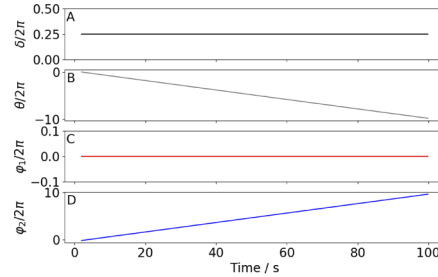

Fig. 5. Calculated outcomes for a circularly-polarised beam through a rotating $\lambda/4$ waveplate ($\Delta\theta = -20\pi$ in 100 s) when no further birefringence is added after the rotating waveplate. Panels A to C: δ, θ, and φ expected for optical hybrid-based detection. Panel D: phase expected for a single photodiode.

This experiment could not be realised in practice, as the patchcords placed after the rotating element add some fixed birefringence which is not a priori known and cannot be set precisely. According to Eq. (12), the output field polarization varies as the $\lambda/4$-waveplate rotates. Depending on the optical field polarization, the fixed birefringence added by the patchcords has a different impact. This did not happen in the previous experiment, as the field polarization remained

circular after the rotating $\lambda/2$-waveplate. To interpret the measurement results we calculated the output field in presence of a rotating $\lambda/4$-waveplate describing $\Delta\theta = -20\pi$ in 100 s, followed by a fixed birefringent element characterised by angles δ_2 and θ_2. Then, we calculated the response of the optical hybrid and a single photodiode for several configurations of δ_2 and θ_2. All simulated outputs can be ascribed to few recurrent behaviours. Particularly, the slave lasers accumulate one of the following phases: 0, $\pm\Delta\theta$, or $\pm2\Delta\theta$. This feature manifests with both detection schemes, although for different values of δ_2 and θ_2. In addition, over-imposed to the linear trend, some variability is observed as the wave-plate rotates, whose amplitude depends on the values assumed by δ_2 and θ_2. Figure 6 shows the calculated outputs and the different phase gains accumulated by the two detection schemes for some particular configurations.
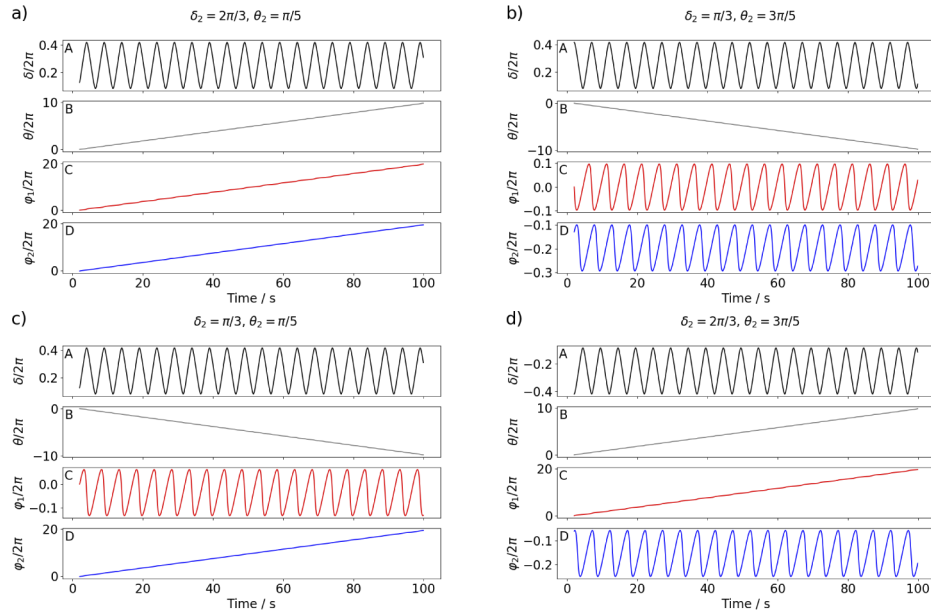

Fig. 6. Calculated outcomes for a circularly-polarised beam through a rotating $\lambda/4$ waveplate ($\Delta\theta = -20\pi$ in 100 s) followed by a fixed birefringent element described by δ_2 and θ_2. Panel legend similar to Fig. 5.

Figure 7 shows the measured outputs for different experimental configurations. In all acquisitions, the $\lambda/4$ waveplate was rotated at constant speed over 10 complete turns ($\Delta\theta = -20\pi$). Between each of the shown measurements, we changed the polarization of the following fiber patch with a manual polarization controller. The exact birefringence introduced by the manual controller could not be measured with our setup, therefore a quantitative prediction of the expected output for each configuration was not possible. Nevertheless, by comparing Fig. 6 and Fig. 7 it can be seen that the obtained results effectively reproduce the expected behaviour.

These tests represent an important validation of the model we assumed for the fiber birefringence and the two types of detection. In addition, they allow quantification of birefringence-induced phase noise, which is often difficult to separate from other noise sources in a metrological measurement.

We stress that for the latter experiment, the manual polarization controller had to be set in a position ensuring sufficient SNR for the photodiode-based detection as the $\lambda/4$-waveplate was rotated. This was not always possible, leading to unlocks of Slave Laser 2. Instead, the PLL of Slave Laser 1, based on the optical hybrid, maintained lock regardless of the waveplate rotation.
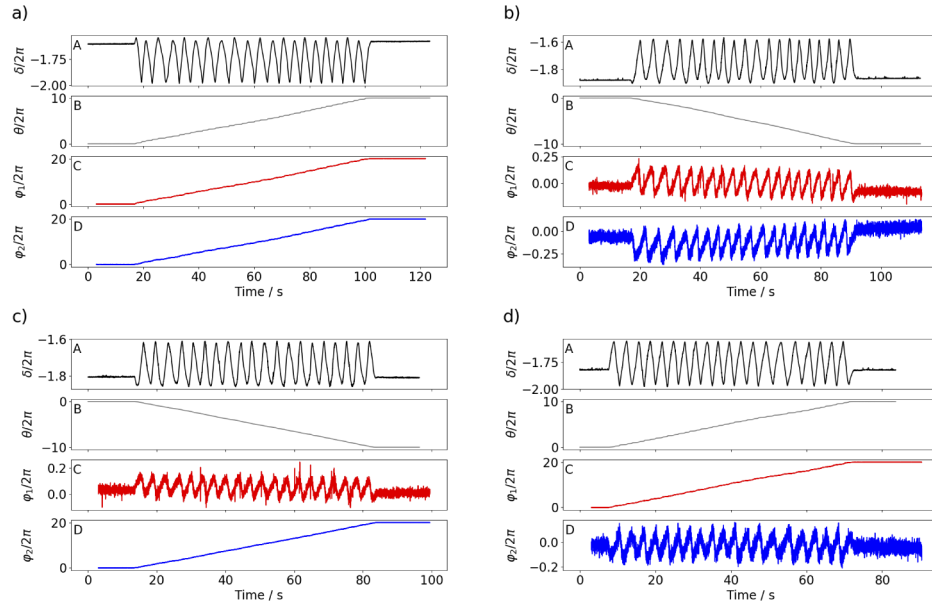
Fig. 7. Experimental results obtained with a circularly-polarised beam through a rotating $\lambda/4$ waveplate ($\Delta\theta = -20\pi$). Panels A (black) and B (gray): δ and θ retrieved with the optical hybrid; C (red): phase of the out-of-loop beatnote between Master Laser and Slave Laser 1, locked to the incoming light using the optical hybrid; D (blue): phase of the out-of-loop beatnote between Master Laser and Slave Laser 2, locked to the incoming light using a single photodiode. Between acquisitions the polarization of the fiber patch after the waveplate was modified with a manual controller.

4.3. Phase detection with an optical-hybrid on an in-field fiber

We connected our setup to the 50 km-long in-field fiber and compared the performances of the two detection schemes when we randomly varied the fiber birefringence by acting on the manual polarization controller. As birefringence was modified, the power and SNR of the beatnotes on the photodiode and optical hybrid used for the PLLs at remote site varied by over 30 dB. Figure 8(a) shows the results obtained with the two detection schemes: the shadowed areas indicate the moments when the SNR at detection was <30 dB in a 100 kHz resolution bandwidth, which is considered as a least requirement to avoid cycles slips. With a single photodiode, cycles slips occurred when the SNR dropped below this threshold. They can be recognised as discrete, random steps in φ_2; finally the laser lost lock and was manually relocked after adequate SNR was recovered. On the contrary, the lock performed with the optical hybrid remained stable and cycles-slips-free even when the SNR in a 100 kHz bandwidth was <30 dB on two of the four photodiodes. In fact, the optical hybrid can always rely on at least two beatnotes having sufficient SNR, ensuring proper tracking of the optical phase in any operating condition. This is an evident experimental proof of the advantage of our proposed solution over the traditional single-photodiode approach.

The power spectral density of the phase difference between Slave Laser 1 and the Master laser is shown in Fig. 8(b) both with (red line) and without (magenta line) noise cancellation. The same measurements are shown for Slave Laser 2 (blue and cyan lines). When the fiber is stabilised, a slight increase in the noise is observed for both slave lasers around 1 kHz, which corresponds to the locking bandwidth of the fibre-stabilisation loop. However, no difference is observed between the two detection approaches within the locking bandwidth of the slave lasers, indicating
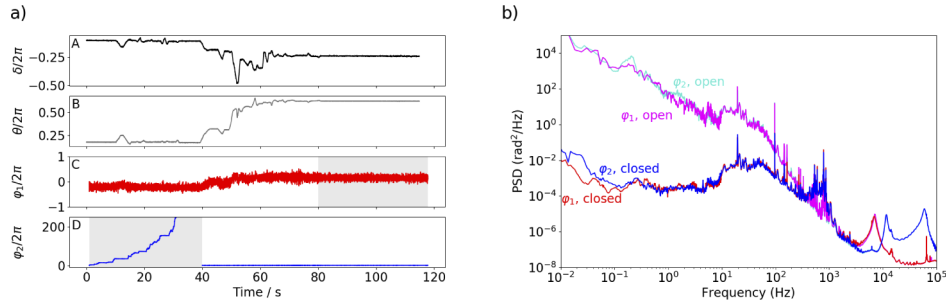
Fig. 8. Experimental results obtained on the metropolitan fiber when the SNR at detection was manually varied by changing the fiber birefringence. (a) Panel legend similar to Fig. 4. Shaded areas on panel C (D) indicate the moments when the SNR at detection was <30 dB in 100 kHz bandwidth on two of the optical hybrid photodiodes (on the single photodiode). (b) The phase noise spectral density of Slave Laser 1 when the fiber is free-running (magenta line) or phase-stabilised (red line) and the same measurement for Slave Laser 2 (cyan and blue line, respectively).

the low-noise phase-tracking capability of the optical hybrid also in a real-field environment. Incidentally, it can be seen that the optical-hybrid-based servo has a locking bandwidth of about 5 kHz, one order of magnitude lower than the analog PLL. This is limited by the current latency of the FPGA, and will be increased in a future upgrade of the digital signal processing. Notably, the residual phase noise of the optical hybrid-based lock does not increase when the relative power of the x / y components is varied. On the contrary, with a single photodiode, the phase coherence is considerably degraded by cycles slips when insufficient SNR is provided to the detection stage.

Figure 9(a) shows the results obtained for the two PLLs over 1 day. In addition, we also show (Panel E) the phase detected by channel 1 of the optical hybrid on a dead-time-free phase counter, $\varphi(I_1)$. As explained in Sec. 4.1, this measurement represents the upper limit to the instability contribution of birefringence-induced effects, phase computation using the FPGA, and locking electronics on the metropolitan fiber loop. As expected, in stationary conditions and in absence of intervention, the polarization changes slowly. The signature of air conditioning inside our laboratory, with a cycle time of ≈ 500 s, is clearly visible on all traces, as it affects both the phase and polarization of optical signals. The evolution of the signal's polarization state can be visualized using the Poincaré sphere representation. This is a three-dimensional coordinate system where reference axes are defined as combinations of the optical field components (E_x, E_y) as follows: $Q = \mathfrak{R}E_x^2 + \mathfrak{I}E_x^2 - \mathfrak{R}E_y^2 - \mathfrak{I}E_y^2$, $U = 2(\mathfrak{R}E_x\mathfrak{R}E_y + \mathfrak{I}E_x\mathfrak{I}E_y)$, $V = 2(\mathfrak{I}E_x\mathfrak{R}E_y - \mathfrak{R}E_x\mathfrak{I}E_y)$. Results for our experiment are shown in Fig. 9(b) [29]. Here, North-South poles of the sphere (Q=0,U=0,V=±1) represent circular polarization for the analysed field, while the U-Q equator represents linear polarization. In particular, a field polarised along the x axis has coordinates (Q=1,U=1,V=0), while a field polarised along the y axis has coordinates (Q=−1,U=1,V=0).

The residual instability of the two slave lasers is shown in Fig. 9(c). The results can be compared to those obtained using a single channel of the optical hybrid. Both optical hybrid and single photodiode detection show similar performances. A comparison of the curves showing the instability of the out-of-loop beatnote between the Master Laser and Slave Laser 1 (φ_1) and the in-loop phase measurement obtained with a single photodiode of the optical hybrid ($\varphi(I_1)$) quantifies the contribution of the short fibers of the interferometer which are not phase-stabilised, in agreement with the measurements shown in Fig. 3. The peak of instability observed at 250 s, indicating a periodic phenomenon synchronous with the cycle time of our air conditioning system, is attributed to the same reason. We observed that the instability at τ=250 s averaging
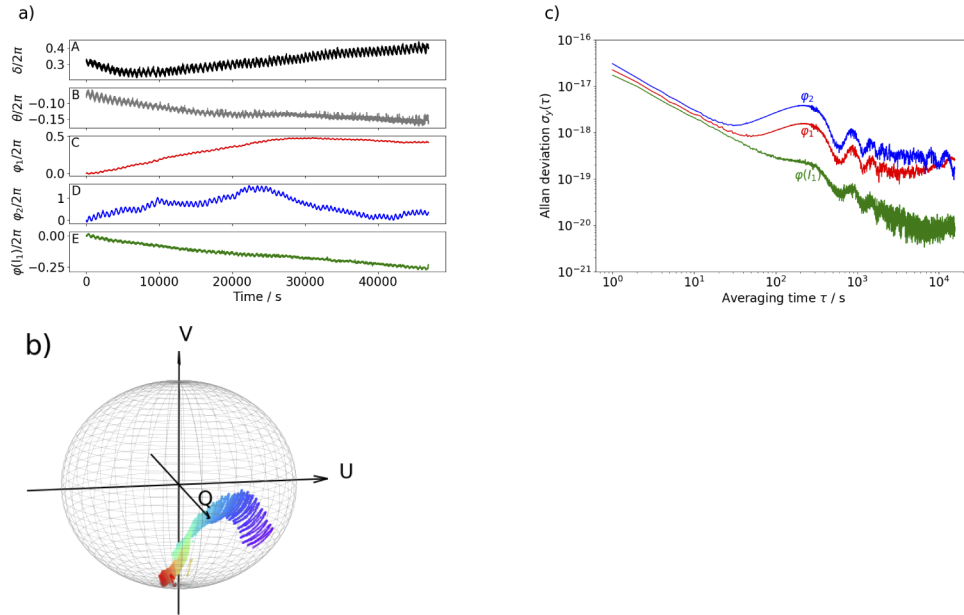
Fig. 9. (a) Panel A to D, legend similar to Fig. 4; panel E (green line) the phase of a single channel of the optical hybrid, $\varphi(I_1)$. (b) The evolution of the signal's polarization state over time (from red to blue) in the Poincaré sphere representation. (c) The relative frequency instability, expressed as the Allan deviation, of the beatnote between the Master Laser and Slave Laser 1 (φ_1, red line) or Slave Laser 2 (φ_2, blue line) and the instability observed on a single channel of the optical hybrid ($\varphi(I_1)$, green line).

time raises from 1×10^{-18} to $\sim 2.5 \times 10^{-18}$ when a 1 m fiber is inserted in the unstabilised paths of the interferometer. This indicates that small differences between the two PLLs can be due to a different sensitivity of the related interferometer branches to temperature changes. An ultimate instability at the 10^{-19} level can be achieved with both approaches.

From time to time, we manually shook the fibers, making the polarization state of the optical field change significantly and rapidly. In occurrence of such non-stationary events the photodiode-based lock had been observed to fail, while the optical hybrid-based lock was not affected. This represents a major advantage of the optical-hybrid-based detection.

5. Conclusion

We propose the use of an optical hybrid as a tool for the polarization state analysis of an optical signal transmitted through a fiber and for continuous tracking of its phase. Such a device is already in use in optical communication systems, although with different tasks, and is based on the simultaneous detection of the different components of the optical field on four photodiodes. By combining the signal from the four of them, it is possible to reconstruct phase and polarization of the received field.

We developed a model to predict its behaviour and a dedicated algorithm that allows extraction of the phase information based on the photodiode readings. This model was validated with specific tests, which also enabled to quantify the impact of polarization-induced phase noise in metrological links for frequency dissemination. We stress that such noise is not related to the adopted detection scheme, but reflects an ambiguity which is intrinsic to the physics of the system. Hence, it is not compensated by the Doppler noise stabilisation technique and sets the ultimate performances which can be achieved. Although a broad literature analysed the problem

of birefringence in optical fibers from a theoretical point of view, this is the first time, to our knowledge, where the effect of polarization-induced phase noise is shown experimentally in a metrological context.

We then used the optical hybrid in a frequency dissemination setup, to phase-lock a regeneration laser to a fiber-delivered reference signal. Our measurements show not only that this device allows low-noise tracking of the optical phase in stationary conditions, but also that tracking is maintained in occurrence of fast flips of the polarization state of the fiber-delivered signal. This is perhaps the most important feature of such an approach, and is a major achievement towards the long term operation of metrological optical links, enabling their full exploitation in many scientific applications.

We plan to upgrade our recently-developed optical fiber backbone in Italy with this kind of detection, to increase the reliability of the dissemination chain. We also envisage its possible use for improving strain and vibration sensing techniques over fiber, as well as in the calibration of apparatus for in-field quantum key distribution protocols [30].

The proposed experiment shows that strong interaction is possible between the fields of telecommunication and optical frequency metrology. The latter has nowadays demonstrated a number of techniques which could be uptaken by telecommunication technology especially in view of increasing the network capacity, such as sub-hertz-linewidth lasers and coherent phase-transfer. On the other hand, a number of photonic devices initially developed for telecommunication technology may improve reliability and performance of metrological links. The use of the optical hybrid is an example of how fruitful such interaction can be.

Funding

Acknowledgments

Disclosures

The authors declare no conflicts of interest.

References

1. C. Lisdat, G. Grosche, N. Quintin, C. Shi, S. M. F. Raupach, C. Grebing, D. Nicolodi, F. Stefani, A. Al-Masoudi, S. Dörscher, S. Häfner, J.-L. Robyr, N. Chiodo, S. Bilicki, E. Bookjans, A. Koczwara, S. Koke, A. Kuhl, F. Wiotte, F. Meynadier, E. Camisard, M. Abgrall, M. Lours, T. Legero, H. Schnatz, U. Sterr, H. Denker, C. Chardonnet, Y. Le Coq, G. Santarelli, A. Amy-Klein, R. Le Targat, J. Lodewyck, O Lopez, and P.-E. Pottie, "A clock network for geodesy and fundamental science," Nat. Commun. **7**(1), 12443 (2016).
2. P. Delva, J. Lodewyck, S. Bilicki, E. Bookjans, G. Vallet, R. Le Targat, P. E. Pottie, C. Guerlin, F. Meynadier, C. Le Poncin-Lafitte, O. Lopez, A. Amy-Klein, W. K. Lee, N. Quintin, C. Lisdat, A. Al-Masoudi, S. Dörscher, C. Grebing, G. Grosche, A. Kuhl, S. Raupach, U. Sterr, I. R. Hill, R. Hobson, W. Bowden, J. Kronjäger, G. Marra, A. Rolland, F. N. Baynes, H. S. Margolis, and P. Gill, "Test of special relativity using a fiber network of optical clocks," Phys. Rev. Lett. **118**(22), 221102 (2017).
3. J. Grotti, S. Koller, S. Vogt, S. Hafner, U. Sterr, C. Lisdat, H. Denker, C. Voigt, L. Timmen, A. Rolland, F. N. Baynes, H. S. Margolis, M. Zampaolo, P. Thoumany, M. Pizzocaro, B. Rauf, F. Bregolin, A. Tampellini, P. Barbieri, M. Zucco, G. A. Costanzo, C. Clivati, F. Levi, and D. Calonico, "Geodesy and metrology with a transportable optical clock," Nat. Phys. **14**(5), 437–441 (2018).

4. T. Takano, M. Takamoto, I. Ushijima, N. Ohmae, T. Akatsuka, A. Yamaguchi, Y. Kuroishi, H. Munekane, B. Miyahara, and H. Katori, "Geopotential measurements with synchronously linked optical lattice clocks," Nat. Photonics **10**(10), 662–666 (2016).
5. C. Clivati, G. Cappellini, L. F. Livi, F. Poggiali, M. Siciliani de Cumis, M. Mancini, G. Pagano, M. Frittelli, A. Mura, G. A. Costanzo, F. Levi, D. Calonico, L. Fallani, J. Catani, and M. Inguscio, "Measuring absolute frequencies beyond the GPS limit via long-haul optical frequency dissemination," Opt. Express **24**(11), 11865 (2016).
6. R. Santagata, D. B. A. Tran, B. Argence, O. Lopez, S. K. Tokunaga, F. Wiotte, H. Mouhamad, A. Goncharov, M. Abgrall, Y. Le Coq, H. Alvarez-Martinez, R. Le Targat, W. K. Lee, D. Xu, P.-E. Pottie, B. Darquié, and A. Amy-Klein, "High-precision methanol spectroscopy with a widely tunable SI-traceable frequency-comb-based mid-infrared QCL," Optica **6**(4), 411 (2019).
7. L. F. Livi, G. Cappellini, M. Diem, L. Franchi, C. Clivati, M. Frittelli, F. Levi, D. Calonico, J. Catani, M. Inguscio, and L. Fallani, "Synthetic dimensions and spin-orbit coupling with an optical clock transition," Phys. Rev. Lett. **117**(22), 220401 (2016).
8. C. Clivati, R. Ambrosini, T. Artz, A. Bertarini, C. Bortolotti, M. Frittelli, F. Levi, A. Mura, G. Maccaferri, M. Nanni, M. Negusini, F. Perini, M. Roma, M. Stagni, M. Zucco, and D. Calonico, "A VLBI experiment using a remote atomic clock via a coherent fiber link," Sci. Rep. **7**(1), 40992 (2017).
9. P. Krehlik, L. Buczek, J. Kolodziej, M. Lipinski, L. Sliwczynski, J. Nawrocki, P. Nogas, A. Marecki, E. Pazderski, P. Ablewski, M. Bober, R. Ciurylo, A. Cygan, D. Lisak, P. Maslowski, P. Morzynski, M. Zawada, R. Campbell, and J. Pieczerak, "Fibre-optic delivery of time and frequency to VLBI station," Astron. Astrophys. **603**, A48 (2017).
10. Y. He, K. G. H. Baldwin, B. J. Orr, R. B. Warrington, M. J. Wouters, A. N. Luiten, P. Mirtschin, T. Tzioumis, C. Phillips, J. Stevens, B. Lennon, S. Munting, G. Aben, T. Newlands, and T. Rayner, "Long-distance telecom-fiber transfer of a radio-frequency reference for radio astronomy," Optica **5**(2), 138 (2018).
11. G. Marra, C. Clivati, R. Luckett, A. Tampellini, J. Kronjaeger, L. Wright, A. Mura, F. Levi, S. Robinson, A. Xuereb, B. Baptie, and D. Calonico, "Ultrastable laser interferometry for earthquake detection with terrestrial and submarine cables," Science **361**(6401), 486–490 (2018).
12. P. A. M. Williams, W. C. Swann, and N. R. Newbury, "High-stability transfer of an optical frequency over long fiber-optic links," J. Opt. Soc. Am. B **25**(8), 1284 (2008).
13. S. Droste, F. Ozimek, Th. Udem, K. Predehl, T. W. Hansch, H. Schnatz, G. Grosche, and R. Holzwarth, "Optical-Frequency Transfer over a Single-Span 1840 km Fiber Link," Phys. Rev. Lett. **111**(11), 110801 (2013).
14. F. Guillou-Camargo, V. Menoret, E. Cantin, O. Lopez, N. Quintin, E. Camisard, V. Salmon, J.-M. Le Merdy, G. Santarelli, A. Amy-Klein, P.-E. Pottie, B. Desruelle, and C. Chardonnet, "First industrial-grade coherent fiber link for optical frequency standard dissemination," Appl. Phys. B **57**(25), 7203–7210 (2018).
15. D. Xu, W.-K. Lee, F. Stefani, O. Lopez, A. Amy-Klein, and P.-E. Pottie, "Studying the fundamental limit of optical fiber links to the 1e-21 level," Opt. Express **26**(8), 9515–9527 (2018).
16. P. Wcislo, P. Ablewski, K. Beloy, S. Bilicki, M. Bober, R. Brown, R. Fasano, R. Ciurylo, H. Hachisu, T. Ido, J. Lodewyck, A. Ludlow, W. McGrew, P. Morzynski, D. Nicolodi, M. Schioppo, M. Sekido, R. Le Targat, P. Wolf, X. Zhang, B. Zjawin, and M. Zawada, "New bounds on dark matter coupling from a global network of optical atomic clocks," Sci. Adv. **4**(12), eaau4869 (2018).
17. E. L. Buckland and R. W. Boyd, "Electrostrictive contribution to the intensity-dependent refractive index of optical fibers," Opt. Lett. **21**(15), 1117 (1996).
18. J. Wuttke, P. M. Krummrich, and J. Rosch, "Polarization Oscilla-tions in Aerial Fiber Caused by Wind and Power-Line Current," IEEE Photonics Technol. Lett. **15**(6), 882–884 (2003).
19. Y. Park, U. Paek, and D. Y. Kim, "Determination of stress-induced intrinsic birefringence in a single-mode fiber by measurement of the two-dimensional stress profile," Opt. Lett. **27**(15), 1291 (2002).
20. D. Calonico, E. K. Bertacco, C. E. Calosso, C. Clivati, G. A. Costanzo, M. Frittelli, A. A. Godone Mura, N. Poli, D. V. Sutyrin, G. M. Tino, M. E. Zucco, and F. Levi, "High-accuracy coherent optical frequency transfer over a doubled 642-km fiber link," Appl. Phys. B **117**(3), 979–986 (2014).
21. D. Calonico, C. Clivati, A. Mura, A. Tampellini, and F. Levi, "The Italian optical link for time and frequency," *2017 Joint Conference of the European Frequency and Time Forum and IEEE International Frequency Control Symposium (EFTF/IFCS)*, Besancon, 2017, pp. 156–159.
22. P. O. Hedekvist, L. Weddig, and S.-C. Ebenhag, "Analysis and compensation of polarization in an optical frequency transfer through a fiber communication network," *32nd European Frequency and Time Forum (EFTF)*, Torino, Italy April 2018 pp. 253–256.
23. C. K.. Tanizawa and A. Hirose, "Fast tracking algorithm for adaptive compensation of high-speed pmd variation caused by SOP change in milliseconds," IEEE Photonics Technol. Lett. **21**(3), 140–142 (2009).
24. S. J. Savory, "Digital coherent optical receivers: Algorithms and subsystems," IEEE J. Sel. Top. Quantum Electron. **16**(5), 1164–1179 (2010).
25. C. B. Czegledi, M. Karlsson, E. Agrell, and P. Johannisson, "Polarization Drift Channel Model for Coherent Fibre-Optic Systems," Sci. Rep. **6**(1), 21217 (2016).
26. R. C. Jones., "A new calculus for the treatment of optical systems. description and discussion of the calculus," J. Opt. Soc. Am. **31**(7), 488–493 (1941).
27. P. K. A. Wai and C. R. Menyuk, "Polarization mode dispersion, decorrelation, and diffusion in optical fibers with randomly varying birefringence," J. Lightwave Technol. **14**(2), 148–157 (1996).

28. C. Clivati, D. Calonico, C. E. Calosso, G. A. Costanzo, F. Levi, A. Mura, and A. Godone, "Planar-Waveguide External Cavity Laser Stabilization for an Optical Link With 10(-19) Frequency Stability," IEEE Trans. Ultrason. Ferroelectr. Freq. Control. **58**(12), 2582–2587 (2011).
29. M. Born and E. Wolf, *Principles of Optics, 7th edition*, (Cambridge University ISBN 0-521-64222-1, 1999).
30. M. Lucamarini, Z. L. Yuan, J. F. Dynes, and A. J. Shields, "Overcoming the rate-distance limit of quantum key distribution without quantum repeaters," Nature **557**(7705), 400–403 (2018).